NANO LETTERS
Letter
pubs.acs.org/NanoLett

The Electric Field of CO Tips and Its Relevance for Atomic Force Microscopy

Michael Ellner,[†] Niko Pavliček,*[,‡] Pablo Pou,[†,§] Bruno Schuler,[‡] Nikolaj Moll,[‡] Gerhard Meyer,[‡] Leo Gross,[‡] and Rubén Peréz*[,†,§]

[†]Departamento de Física Teórica de la Materia Condensada, Universidad Autónoma de Madrid, E-28049 Madrid, Spain
[‡]IBM Research−Zurich, 8803 Rüschlikon, Switzerland
[§]Condensed Matter Physics Center (IFIMAC), Universidad Autónoma de Madrid, E-28049 Madrid, Spain

Supporting Information

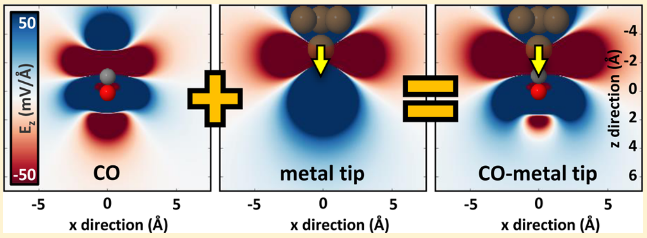

ABSTRACT: Metal tips decorated with CO molecules have paved the way for an impressively high resolution in atomic force microscopy (AFM). Although Pauli repulsion and the associated CO tilting play a dominant role at short distances, experiments on polar and metallic systems show that electrostatic interactions are necessary to understand the complex contrast observed and its distance evolution. Attempts to describe those interactions in terms of a single electrostatic dipole replacing the tip have led to contradictory statements about its nature and strength. Here, we solve this puzzle with a comprehensive experimental and theoretical characterization of the AFM contrast on Cl vacancies. Our model, based on density functional theory (DFT) calculations, reproduces the complex evolution of the contrast between both the Na cation and Cl anion sites, and the positively charged vacancy as a function of tip height, and highlights the key contribution of electrostatic interactions for tip−sample distances larger than 500 pm. For smaller separations, Pauli repulsion and the associated CO tilting start to dominate the contrast. The electrostatic field of the CO−metal tip can be represented by the superposition of the fields from the metal tip and the CO molecule. The long-range behavior is defined by the metal tip that contributes the field of a dipole with its positive pole at the apex. At short-range, the CO exhibits an opposite field that prevails. The interplay of these fields, with opposite sign and rather different spatial extension, is crucial to describe the contrast evolution as a function of the tip height.

KEYWORDS: *Non-contact atomic force microscopy, tip functionalization, high-resolution imaging, CO molecule, contrast mechanisms, DFT*

Frequency modulation atomic force microscopy (FM-AFM) has been recognized for a long time as one of the best tools for materials characterization at the atomic scale. The use of metal tips decorated with CO molecules represented a significant step forward in this technique that paved the way for the visualization of the internal structure of molecules with unprecedented resolution.[1] The contrast enhancement provided by these functionalized tips has made possible to unveil the molecular structure of natural compounds[2] and small metallic clusters,[3] to follow the intermediate states of chemical reactions,[4,5] and, even, to visualize the subtle changes in charge density and bond length associated with the bond order of covalent bonds.[6] CO tips also act as a force-to-current transducer,[7] achieving atomic resolution with scanning tunneling hydrogen microscopy[8] (STHM) and with inelastic electron tunneling spectroscopy[9] (IETS). CO tips also increase the resolution in Kelvin probe force microscopy (KPFM).[10]

The high resolution achieved by the CO-terminated tips (CO tips) has been explained in terms of strong Pauli repulsion between the closed-shell molecule acting as the probe and the electronic charge of the molecule probed.[1,11] In addition, the associated tilting of the CO molecule[6,12−14] amplifies the spatial variations of the charge density on the sample. Although Pauli repulsion plays a dominant role at very close distances, recent experiments on polar molecules,[15−18] ionic samples,[19] and metallic surfaces,[3] consistently show that other interactions, in particular electrostatic forces, are also relevant to understand the complex observed contrast.

The consensus ends here as the recent literature includes contradictory statements about the nature of the charge distribution of the CO molecule when acting as a tip or probed as an adsorbate. In the gas phase, CO has a total electric dipole of ~0.12 D with its positive pole pointing to the oxygen. However, a CO tip dipole with its negative pole at the O atom (hereinafter called negative dipole) has been invoked by Schneiderbauer et al.[19] to explain atomic corrugation in AFM measurements with a CO tip on an ionic copper nitride (Cu_2N) surface. The presence of a negative charge at the

Received: December 23, 2015
Revised: January 27, 2016
Published: February 3, 2016

DOI: 10.1021/acs.nanolett.5b05251
Nano Lett. 2016, 16, 1974−1980

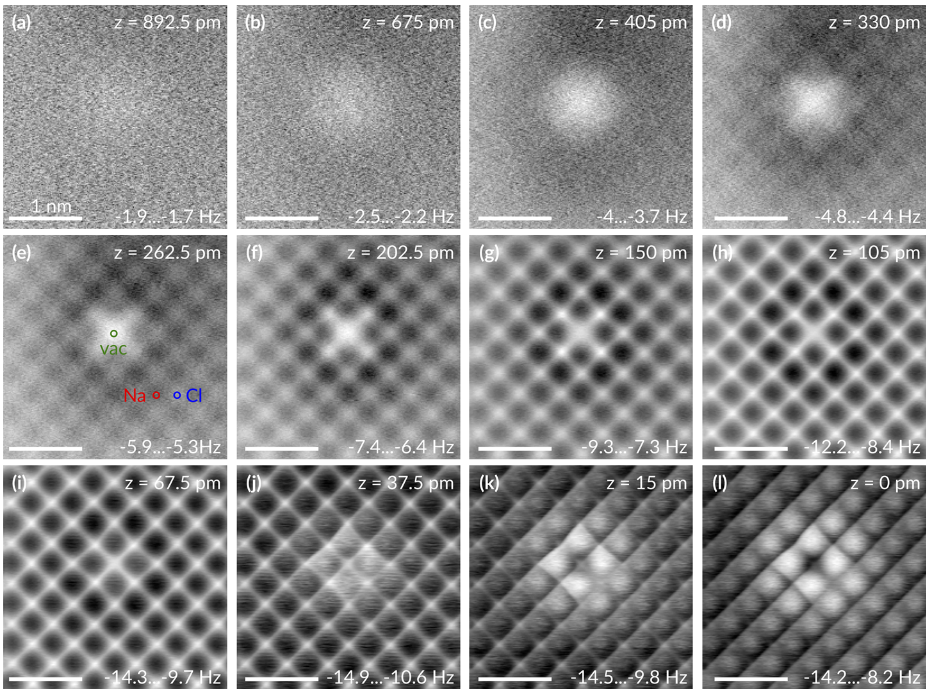

Figure 1. Experimental constant-height AFM measurements of a Cl vacancy in bilayer NaCl on Cu(111) acquired with a CO tip. The tip height z, indicated in the top right, decreases from (a) to (l). $z = 0$ is defined as the distance at closest approach, corresponding to the data shown in (l). The frequency shift limits corresponding to black (more negative) and white are indicated in the bottom right of each panel. The positions of the vacancy site (vac, green), the Na site (Na, red), and the Cl site (Cl, blue) are indicated in panel (e). Scale bars correspond to 1 nm.

oxygen in CO tips is also supported by Hapala et al.[16] in their analysis of AFM, STM, and IETS images of Co phthalocyanines. Contrary to this, Schwarz et al.[20] explain the contrast formation of individual CO molecules adsorbed on different metal surfaces probed with a metal tip by assuming that the adsorbed CO molecules have a small dipole with its positive pole at the O atom (as in the gas phase, hereinafter called positive dipole). The dipole orientation is not even consistent among studies of the CO molecule as an adsorbate, as Hofmann et al.[21] explain their measurements for CO on a Cu surface with the negative pole on the oxygen, just the opposite of the proposal reported in refs 20 and 22 when studying the same system.

It is clear that further advances in high-resolution imaging with CO tips call for a detailed characterization of the electronic charge distribution of CO−metal apexes and its contribution to the AFM contrast. Cl vacancies in the top layer of NaCl(100), which have already been extensively studied using both STM and AFM,[23−26] provide an ideal model system for this task. First, these localized ionic defects provide unambiguous lattice site identification. Second, in addition to the ionic lattice, there is a net positive charge at the vacancy site leading to three qualitatively different sites: Na cations (Na^+), Cl anions (Cl^-), and the net positively charged vacancy site. Finally, the atomic lattice and the vacancy are expected to be more robust (than other systems such as adsorbates) against tilting or displacements due to lateral forces during the measurement.

In this Letter, we solve the puzzle regarding the nature of the electrostatic dipole in CO-decorated metal tips and the role played by the different tip−sample interactions with a full characterization of the AFM contrast formation mechanisms in Cl vacancies. We combine experimental AFM measurements with a theoretical model, based on density functional theory (DFT) calculations, that allows an efficient simulation of AFM images while retaining a first−principles accuracy. Our model reproduces the complex evolution of the contrast between the Na^+/Cl^- sites and the positive vacancy as a function of the tip height, and highlights the key contribution of electrostatic interactions for tip−sample distances larger than 500 pm. Pauli repulsion and the associated tip relaxations start to dominate the contrast for closer separations. The electrostatic field of the CO−metal tip can be represented by the sum of a dipole field that takes into account the positive charge accumulation at the metal apex due to the Smoluchowski effect,[27] and the electrostatic field of an isolated CO molecule, that exhibits negative charge accumulation in front of the oxygen atom due to its lone pair. The interplay of these fields, with opposite sign in the near-field and rather different spatial extension, explains the contrast evolution observed in our experiments and reconciles the apparently contradictory claims in the literature.

Results and Discussion. Measurements were performed using a home-built combined STM and AFM operating in ultrahigh vacuum (base pressure below 10^{-10} mbar) at a temperature of 5 K. The voltage V was applied to the sample. The AFM is based on a qPlus sensor[28] (stiffness $k \approx 1800$ N/m, eigenfrequency $f_0 = 29664$ Hz, quality factor $Q \approx 2 \times 10^5$) operated in frequency-modulation mode.[29] The PtIr tip was cut to length and sharpened using a focused ion beam setup. All AFM images were acquired at $V = 0$ V to avoid any cross-talk of the current and force signals and which was also within a few 100 mV of the local contact potential difference.[24] The oscillation amplitude was 50 pm to maximize the lateral resolution on atomic length scales.[30]

A Cu(111) single crystal was cleaned by several sputtering and annealing cycles. Ultrathin NaCl films were grown by thermal evaporation of NaCl on Cu(111) at a sample temperature of about 270 K. Defect-free (100)-terminated

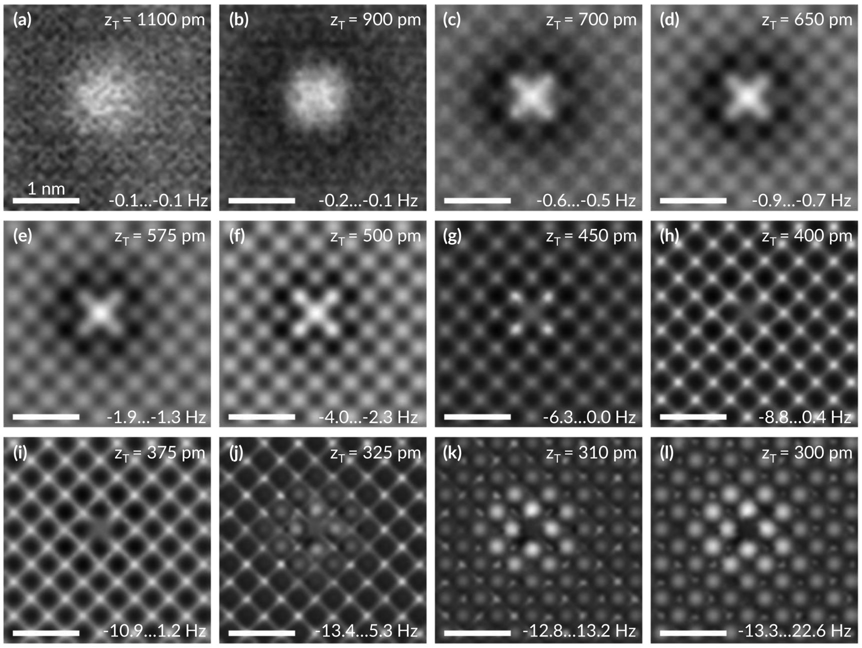

Figure 2. Theoretical AFM images of a Cl vacancy in bilayer NaCl on Cu(100) using a CO probe and a 1.5 D dipole simulating a Cu tip. The tip height z_T, indicated in the top right, decreases from (a) to (l). The frequency shift limits corresponding to black (more negative) and white are indicated in the bottom right of each panel. Scale bars correspond to 1 nm.

islands of mainly two atomic layers were formed.[31] Low coverages of CO molecules were adsorbed at sample temperatures below 10 K.

To create a single Cl vacancy in the top layer of bilayer NaCl on Cu(111), a sharp Cu tip was approached by about 0.5 nm at zero voltage from an STM set-point current of I = 2 pA at a voltage of V = 0.2 V. Thereby a single Cl atom is transferred from the surface to the tip leading to a characteristic contrast change. A sharp Cu tip is then re-established by bringing the tip into contact with the bare Cu(111) surface. Consecutively, a CO tip was prepared by picking up a single CO molecule from NaCl.[1] The Cl vacancy can be unambiguously identified by its characteristic features in STS,[23] by KPFM,[24] or by atomically resolved STM[23,25] and AFM images.[26]

Figure 1 presents experimental AFM raw data of a Cl vacancy acquired with a CO tip as a function of tip−sample distance. We accounted for potential drift in the z direction by switching on the STM feedback loop for a short time after each image. The distance has been varied by nearly 0.9 nm, and the tip height corresponding to the closest approach has been defined as z = 0. From the data, we can distinguish four distinctly different distance regimes each leading to specific contrast. For large tip heights ($z \sim$ 900−400 pm) (Figures 1a−c), only the vacancy can be resolved as a faint and broad feature of less negative frequency shift. For $z \sim$ 400−200 pm (Figures 1d−f), atomic corrugation on the ionic lattice gradually emerges, with the Cl^- (Na^+) lattice sites leading to less (more) negative frequency shift. The vacancy site remains the feature of least negative frequency shift, but the contrast compared to the surrounding Cl sites decreases with tip approach until it disappears at $z \sim$ 200 pm. For smaller tip—sample distances, sharp bright ridges arise (Figures 1g−j) connecting neighboring Cl sites and also the vacancy site with its four neighboring Cl sites. Finally, for tip heights below $z \sim$ 20 pm, (Figures 1k−l), the atomic contrast reverses, both on the ionic lattice and the vacancy. The vacancy becomes the darkest site (most negative frequency shift), while the Na sites are now the brightest features (least negative frequency shift), separated by a sharp, dark Cl grid.

We have rationalized the experimental findings by a model based on density functional theory (DFT) calculations, which allows an efficient simulation of AFM images while retaining the first−principles accuracy needed to cover the whole distance range explored in the experiments, and to single out the different contributions to the total tip−sample interaction. Our approach differs from previous theoretical models[12,16] in two important aspects. We go beyond the simple dipole approximation for the CO probe and calculate the electrostatic energy by the interaction of the sample electrostatic potential (obtained from a DFT calculation) with the charge density of both the CO molecule (also calculated with DFT) and the metal tip apex (replaced by a positive dipole). We also include a more accurate description of the short-range (SR) interaction, that is modeled as a sum of pairwise Morse potentials with Cl/Na species-dependent parameters fitted to reproduce our DFT force calculations (see the Supporting Information for details). The van der Waals (vdW) contributions are included with a semiempirical DFT-D3 approach,[32] while the CO tilting is simulated by a spring[12] with a force constant of 0.24 N/m[18] (see Figure S3 in the Supporting Information).

DFT calculations have been carried out with VASP[33] using a periodic supercell approach and the PBE[34] exchange-correlation functional supplemented with the same semi-empirical DFT-D3 description of vdW interactions used in the model. We have used a 400 eV cutoff for the plane-wave basis set, PAW pseudopotentials, and include dipole corrections to cancel the spurious interaction between neighboring cells. DFT force calculations at Na, Cl, bridge atomic positions of the clean NaCl/Cu(100) surface and an isolated CO molecule acting as a probe were taken as the reference data to fit the Morse potentials, once the vdW and electrostatic terms were subtracted from the DFT energy (see Figure S1).

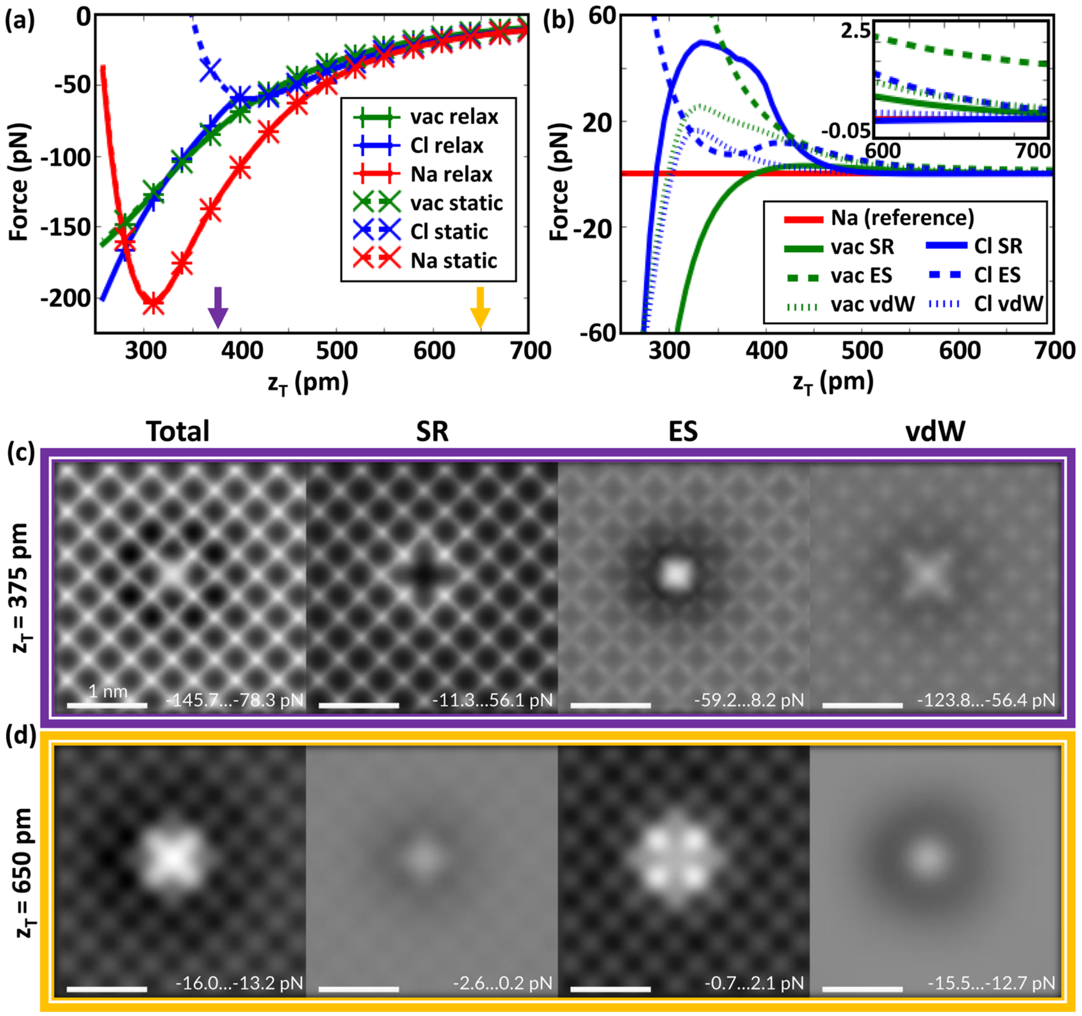

Figure 3. (a) Total force with (solid) and without (dashed lines) relaxation of the CO probe for the vacancy (green), Cl (blue), and Na (red) sites. (b) Force decomposed spectroscopy for the above sites in terms of short-range (SR, solid), electrostatic (ES, dashed), and van der Waals (vdW, dotted lines) interaction. Force decomposed images in terms of the above-mentioned interactions for (c) z_T = 375 pm and (d) z_T = 650 pm. In order to highlight the influence of each contribution on the total force, the gray scale in all of the images corresponds to the *variation range* of the *total* force. For the large tip−sample distances (z_T > 450 pm) the main contribution of the total force comes from the electrostatic interaction, while for small distances, the main contribution for the Na/Cl contrast comes from the SR interaction and for the vacancy from the electrostatics.

We have applied the model to a single Cl vacancy on a 6 × 6 surface unit cell (see Figure S2) using a slab composed of a NaCl(100) bilayer and 2 Cu(100) layers and a large vacuum region (total cell size 33.7 Å × 33.7 Å × 49 Å). Figure 2 shows calculated images for a range of tip heights z_T—defined as the distance of the O atom of the tip to the topmost atomic NaCl layer—corresponding to those in Figure 1. We obtained excellent qualitative and quantitative agreement with the experiment, reproducing the contrast at every site (vacancy, Na, and Cl atoms close and far from the vacancy) and the contrast changes as a function of the tip height. By comparison to the experiment, we can relate the experimental height scale z to the absolute tip−sample distances z_T with an offset of 300 pm: $z = z_T - 300$ pm.

Contrast changes with tip height arise from the variation of the relative weight of the short-range (SR), electrostatic (ES), and vdW contributions to the total tip−sample interaction. Figure 3 illustrates the distance dependence of these contributions with force curves on the Na, Cl, and vacancy sites (marked in Figure 1e), and 2D force maps at two characteristic tip−surface distances. The electrostatic force dominates the image contrast for tip heights z_T above 500 pm. Figure 3b shows that the electrostatic contribution to the force contrast (force differences among sites) remains larger than the SR one for tip heights larger than 450 pm. This change in the force contrast is responsible for the contrast change in the images observed at 500 pm in Figure 2, as the frequency shift is proportional to the derivative of forces (Figure S4). The electrostatic force is responsible for the bright (less attractive) broad feature associated with the positively charged vacancy at large tip heights (Figure S5), and for the atomic contrast that emerges in the medium tip height regime ($z_T \sim 700-500$ pm). In this distance range, the positive Na sites show a larger negative frequency shift (i.e., a more attractive interaction) than the negative Cl sites, while the positive vacancy site remains the least attractive site (Figures 3b and d). Thus, the tip apparently exhibits the behavior of a negative dipole on Na/Cl, but that of a positive dipole on the vacancy site, highlighting the limitations of the common dipole approximation to describe the electric field created by the tip (see the discussion below).

For small tip heights (z_T < 500 pm), the SR interaction becomes the most important contribution to the contrast due

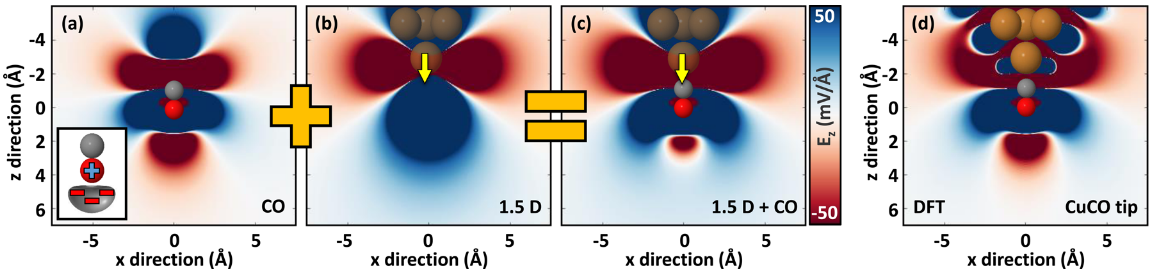

Figure 4. *z*-component of the electric field E_z of (a) a CO probe, (b) a 1.5 D dipole moment modeling a Cu metal tip, and (c) CO probe plus a 1.5 D dipole moment. The inset in (a) shows a scheme of the CO charge distribution that is responsible for the strongly negative (repulsive for electrons) E_z in front of the O atom. (d) Electric field of a CO–Cu tip as calculated through DFT.

to the exponential growth of the Pauli repulsion above the Cl sites (Figure 3b). At $z_T \sim 400$–375 pm, the CO molecule starts to tilt to avoid the high repulsion over the Cl anions, as shown by the difference between the static and relaxed curves in Figure 3a (see also Figure S5). Notice that, in this distance range, the Na/Cl contrast from the electrostatic contribution is much smaller compared to the SR (Figure 3c). However, on the vacancy site, due to the small electron density, the Pauli repulsion is negligible, and the electrostatic interaction remains dominant. Upon further approach, the CO probe increases its tilting toward the minima of the potential energy surface (PES) (Figure S5), and by doing so, the saddle line between two neighboring Cl ions (and the vacancy and its neighboring Cl ions) is apparently sharpened.[6,12] For the smallest tip heights explored ($z_T \sim 310$–300 pm), the Na sites become brighter than the Cl sites (see Figure 2). This contrast inversion is explained by the change of the slope of the force on the Na sites as it reaches its minimum at $z_T \sim 310$ pm (see Figure 3a). At this tip height, the force still increases with decreasing tip height both on the Cl sites (due to the tip tilting toward the Na atoms) and on the vacancy (due to the small Pauli repulsion).

The rich contrast behavior in the large and medium tip height regimes can only be explained taking into account the charge distribution of the CO tip (see Figure S6). Before addressing this important issue, we have to consider the accuracy of our electrostatic model, where the tip is simulated by the sum of the charge density of the CO molecule obtained from a DFT calculation, and a positive dipole with a magnitude of 1.5 D placed 53 pm outside of the outermost metal atom that represents the metal tip.[22,27] This approximation reflects the fact that the electric field generated by a metallic tip arises from the Smoluchowski effect[27] and can be described by an effective positive dipole.[22] Our approach for the tip is further supported by DFT calculations of the electric field created by a CO molecule attached to a 20-atom Cu tip (see Figure 4d and Figure S7). Our results validate the additivity of the isolated CO and Cu apex systems to describe the electric field[35] and confirm that metallic tips can be simulated by a positive dipole. The best fit for the electric field is actually provided by a dipole moment of 0.7 D (see Figure S7). However, this dipole moment, when incorporated into the model, fails to reproduce the contrast of the vacancy that, according to the experiment, should appear as the brighter feature for distances where the electrostatic interaction dominates (see Figures S8 and S9). The right contrast can be restored with a 1.5 D dipole, that places the contrast change around $z_T = 500$ pm (for larger distances the vacancy appears brighter than the surrounding Cl sites). Several reasons to explain this discrepancy between the calculated and the effective dipole necessary to reproduce the experiments are considered in the Supporting Information, but here we take a practical approach considering the dipole moment representing the metallic tip as a fitting parameter that is validated by the excellent agreement between the theoretical model and the experiment.

We are now in the position to discuss how the interplay of the E_z electric field created separately by the CO and the positive dipole replacing the metal tip (see Figures 4a–c for each of the contributions and the sum) explains the observed contrast for the large and medium tip height regime ($z_T > 500$ pm). In consistence with literature, our DFT calculations show that the total charge distribution of the isolated CO molecule has a small dipole of 0.12 D, with its positive pole at the oxygen. However, the electric field of the molecule is quite complex and can only be replaced by the one created by this small dipole for very large tip–sample distances ($z_T > 1000$ pm). For closer distances, the field is ruled by the local charge distribution. Ahead of the oxygen atom, the electric field is effectively produced by a localized negatively charged cloud in front of this atom neutralized by a positive charge in the nucleus (see the inset of Figure 4a). This charge distribution arises from the asymmetry in the electronic charge density induced by the oxygen lone pair. In the near field, the resulting electric field resembles the one created by a negative dipole placed at the oxygen atom. Thus, the combined electrostatic field of the CO probe and the metal tip can be represented by two opposing dipoles. For the uncompensated positive charge of the vacancy, both dipoles contribute and compensate each other but the larger positive dipole dominates, leading to a repulsion above the vacancy site, already observable at large tip heights (Figure S10). However, in the case of the atomic Na and Cl sites, the rather different spatial extension of the electric fields (see Figure S11) leads to a completely different scenario. The dipole coming from the metal apex cannot resolve those sites because its field spreads out significantly at the sample surface, effectively averaging their opposite contribution. On the contrary, the smaller but rather localized electric field created by the CO molecule is crucial for explaining the observed atomic resolution.

The insight gained from our analysis can be used to address the apparent contradiction in the interpretation of previous experiments involving CO molecules either as a tip on a metallic apex probing ionic surfaces[19] or as an adsorbate probed with a pure metallic tip.[20] Our results show that the electrostatic field of the CO tip is crucial to describe the AFM contrast on the atomic scale. We proved that the simplified description of the tip as a single dipole to explain the electrostatic interactions fails. In addition to the use of different AFM modes and operation parameters, the main reason for the contradictory assignment of the CO dipoles' direction in recent publications[19,20] is probably related to this approximation. Here, we have developed a methodology for the calculation of AFM images including the detailed local charge distributions of the CO tip and obtained excellent agreement with experiments on the model system of Cl vacancies, which exhibit several contrast inversions as a function of tip height.

Conclusions. In summary, we have identified the contrast formation mechanisms for AFM images of localized ionic defects using CO-decorated metal tips. The electrostatic interaction dominates the contrast at large and medium tip—sample distances (>500 pm), while Pauli repulsion takes over at closer separations, where the CO probe tilts and highlights saddle lines as ridges. This electrostatic interaction cannot be described by a tip modeled by a single dipole. It is necessary to take into account both the positive dipole that describes the electric field created by the metal tip and the negative charge cloud strongly localized in front of the oxygen atom. The opposite sign and different spatial extension of the associated electric fields explain the rich contrast observed. While both terms compete to determine the contrast of uncompensated, extended defects like the Cl vacancy, atomic-scale resolution of the ionic lattice arises mainly from the CO electric field as the more extended field created by the metal apex averages out the contribution coming from those periodic and rapidly varying charge distributions. These ideas provide a unified framework that solves the apparent contradictions among previous experiments with CO molecules acting as probes or adsorbates.

■ ASSOCIATED CONTENT

Ⓢ Supporting Information

The Supporting Information is available free of charge on the ACS Publications website at DOI: 10.1021/acs.nanolett.5b05251.

> Additional information on the determination of the tip—sample interaction potential from DFT calculations, the contribution of the different interaction components to the frequency shift images as a function of distance, and the electric field of CO—functionalized metal tips, as well as an additional series of experimental AFM raw data images acquired with a different CO tip (PDF)

■ AUTHOR INFORMATION

Corresponding Authors

*E-mail: pav@zurich.ibm.com.
*E-mail: ruben.perez@uam.es.

Author Contributions

M.E. and N.P. contributed equally to this work.

Notes

The authors declare no competing financial interest.

■ ACKNOWLEDGMENTS

We thank the Marie Curie ITN Networks ACRITAS (FP7-PEOPLE-2012-ITN-317348) and qTea (FP7-PEOPLE-2012-ITN-317485), the Spanish MINECO (projects CSD2010-00024 and MAT2014-54484-P), the ERC Advanced Grant CEMAS (agreement no. 291194), and EU project PAMS (610446) for financial support. Computer time provided by the Spanish Supercomputer Network (RES) at the Marenostrum III (BSC, Barcelona) and Magerit (CesViMa, Madrid) computers. P. P. was supported by the Ramón y Cajal program. We thank R. Allenspach for valuable comments on the manuscript.

■ REFERENCES

(1) Gross, L.; Mohn, F.; Moll, N.; Liljeroth, P.; Meyer, G. *Science* **2009**, *325*, 1110−1114.

(2) Gross, L.; Mohn, F.; Moll, N.; Meyer, G.; Ebel, R.; Abdel-Mageed, W. M.; Jaspars, M. *Nat. Chem.* **2010**, *2*, 821−825.

(3) Emmrich, M.; Huber, F.; Pielmeier, F.; Welker, J.; Hofmann, T.; Schneiderbauer, M.; Meuer, D.; Polesya, S.; Mankovsky, S.; Ködderitzsch, D.; Ebert, H.; Giessibl, F. J. *Science* **2015**, *348*, 308−311.

(4) de Oteyza, D. G.; Gorman, P.; Chen, Y.-C.; Wickenburg, S.; Riss, A.; Mowbray, D. J.; Etkin, G.; Pedramrazi, Z.; Tsai, H.-Z.; Rubio, A.; Crommie, M. F.; Fischer, F. R. *Science* **2013**, *340*, 1434−1437.

(5) Albrecht, F.; Pavliček, N.; Herranz-Lancho, C.; Ruben, M.; Repp, J. *J. Am. Chem. Soc.* **2015**, *137*, 7424−7428.

(6) Gross, L.; Mohn, F.; Moll, N.; Schuler, B.; Criado, A.; Guitián, E.; Peña, D.; Gourdon, A.; Meyer, G. *Science* **2012**, *337*, 1326−1329.

(7) Weiss, C.; Wagner, C.; Kleimann, C.; Rohlfing, M.; Tautz, F. S.; Temirov, R. *Phys. Rev. Lett.* **2010**, *105*, 086103.

(8) Kichin, G.; Weiss, C.; Wagner, C.; Tautz, F. S.; Temirov, R. *J. Am. Chem. Soc.* **2011**, *133*, 16847−16851.

(9) Chiang, C.-l.; Xu, C.; Han, Z.; Ho, W. *Science* **2014**, *344*, 885−888.

(10) Mohn, F.; Gross, L.; Moll, N.; Meyer, G. *Nat. Nanotechnol.* **2012**, *7*, 227−231.

(11) Moll, N.; Gross, L.; Mohn, F.; Curioni, A.; Meyer, G. *New J. Phys.* **2010**, *12*, 125020.

(12) Hapala, P.; Kichin, G.; Wagner, C.; Tautz, F. S.; Temirov, R.; Jelínek, P. *Phys. Rev. B: Condens. Matter Mater. Phys.* **2014**, *90*, 085421.

(13) Boneschanscher, M. P.; Hämäläinen, S. K.; Liljeroth, P.; Swart, I. *ACS Nano* **2014**, *8*, 3006−3014.

(14) Neu, M.; Moll, N.; Gross, L.; Meyer, G.; Giessibl, F. J.; Repp, J. *Phys. Rev. B: Condens. Matter Mater. Phys.* **2014**, *89*, 205407.

(15) Moll, N.; Schuler, B.; Kawai, S.; Xu, F.; Peng, L.; Orita, A.; Otera, J.; Curioni, A.; Neu, M.; Repp, J.; Meyer, G.; Gross, L. *Nano Lett.* **2014**, *14*, 6127−6131.

(16) Hapala, P.; Temirov, R.; Tautz, F. S.; Jelínek, P. *Phys. Rev. Lett.* **2014**, *113*, 226101.

(17) Albrecht, F.; Repp, J.; Fleischmann, M.; Scheer, M.; Ondráček, M.; Jelínek, P. *Phys. Rev. Lett.* **2015**, *115*, 076101.

(18) Weymouth, A. J.; Hofmann, T.; Giessibl, F. J. *Science* **2014**, *343*, 1120−1122.

(19) Schneiderbauer, M.; Emmrich, M.; Weymouth, A. J.; Giessibl, F. J. *Phys. Rev. Lett.* **2014**, *112*, 166102.

(20) Schwarz, A.; Köhler, A.; Grenz, J.; Wiesendanger, R. *Appl. Phys. Lett.* **2014**, *105*, 011606.

(21) Hofmann, T.; Pielmeier, F.; Giessibl, F. J. *Phys. Rev. Lett.* **2014**, *112*, 066101.

(22) Gao, D. Z.; Grenz, J.; Watkins, M. B.; Canova, F. F.; Schwarz, A.; Wiesendanger, R.; Shluger, A. L. *ACS Nano* **2014**, *8*, 5339−5351.

(23) Repp, J.; Meyer, G.; Paavilainen, S.; Olsson, F. E.; Persson, M. *Phys. Rev. Lett.* **2005**, *95*, 225503.

(24) Gross, L.; Schuler, B.; Mohn, F.; Moll, N.; Pavliček, N.; Steurer, W.; Scivetti, I.; Kotsis, K.; Persson, M.; Meyer, G. *Phys. Rev. B: Condens. Matter Mater. Phys.* **2014**, *90*, 155455.

(25) Li, Z.; Chen, H.-Y. T.; Schouteden, K.; Lauwaet, K.; Janssens, E.; Van Haesendonck, C.; Pacchioni, G.; Lievens, P. *ACS Nano* **2015**, *9*, 5318−5325.

(26) Schuler, B.; Persson, M.; Paavilainen, S.; Pavliček, N.; Gross, L.; Meyer, G.; Repp, J. *Phys. Rev. B: Condens. Matter Mater. Phys.* **2015**, *91*, 235443.

(27) Smoluchowski, R. *Phys. Rev.* **1941**, *60*, 661.

(28) Giessibl, F. J. *Appl. Phys. Lett.* **2000**, *76*, 1470−1472.

(29) Albrecht, T.; Grütter, P.; Horne, D.; Rugar, D. *J. Appl. Phys.* **1991**, *69*, 668−673.

(30) Giessibl, F. J. *Rev. Mod. Phys.* **2003**, *75*, 949−983.

(31) Bennewitz, R.; Barwich, V.; Bammerlin, M.; Loppacher, C.; Guggisberg, M.; Baratoff, A.; Meyer, E.; Güntherodt, H.-J. *Surf. Sci.* **1999**, *438*, 289−296.
(32) Grimme, S.; Antony, J.; Ehrlich, S.; Krieg, H. *J. Chem. Phys.* **2010**, *132*, 154104.
(33) Kresse, G.; Furthmüller, J. *Comput. Mater. Sci.* **1996**, *6*, 15−50.
(34) Perdew, J. P.; Burke, K.; Ernzerhof, M. *Phys. Rev. Lett.* **1996**, *77*, 3865.
(35) Sun, Z.; Boneschanscher, M. P.; Swart, I.; Vanmaekelbergh, D.; Liljeroth, P. *Phys. Rev. Lett.* **2011**, *106*, 046104.